Ordering kinetics in two-dimensional hexagonal pattern of cylinder-forming PS-*b*-PMMA block copolymer thin films: Dependence on the segregation strength

Gabriele Seguini,[1,*] Fabio Zanenga,[1,2] Michele Laus,[2] and Michele Perego[1,†]
[1]*Laboratorio MDM, IMM-CNR, Via C. Olivetti 2, I-20864 Agrate Brianza, Italy*
[2]*Dipartimento di Scienze e Innovazione Tecnologica, Università del Piemonte Orientale "A. Avogadro," INSTM, UdR Alessandria, Viale T. Michel 11, I-15121 Alessandria, Italy*

(Received 24 January 2018; revised manuscript received 5 April 2018; published 24 May 2018)

This paper reports the experimental determination of the growth exponents and activation enthalpies for the ordering process of standing cylinder-forming all-organic polystyrene-*block*-poly (methyl methacrylate) block copolymer (BCP) thin films as a function of the BCP degree of polymerization (N). The maximum growth exponent of 1/3 is observed for the BCP with the lowest N at the border of the order-disorder transition. Both the growth exponents and the activation enthalpies exponentially decrease with the BCP segregation strength (χN) following the same path of the diffusivity.

DOI: 10.1103/PhysRevMaterials.2.055605

A two-dimensional (2D) hexagonal lattice (domains with crystalline structure) represents the equilibrium, low-temperature, low-symmetry phase of various spatiality modulated phase systems, i.e., crystalline solids, colloidal systems, and block copolymer (BCP) thin films [1–4]. The size and the number of atoms or colloids are fixed; conversely, in BCPs the size of the domains can deform and their number can change over time. The equilibrium state corresponds to the absolute minimum free energy of the system. The similarities extend to the types of topological defects, disclinations, dislocations, and grain boundaries [5–7]. The Kosterlitz-Thouless-Halperin-Nelson-Young theory describes the 2D melting for a system in complete thermodynamic equilibrium by means of a two-step continuous transition [8–10]. Experimentally, the polycrystalline pattern coarsens in time toward the equilibrium state by annihilation of the topological defects reducing the grain boundary length and by reorientation of ordered domains through thermally activated kinetic processes. The grain size of the hexagonal lattice grows in time (t), scaling as t^{ϕ}, where ϕ is the growth exponent [11,12]. The ordering process is relevant both fundamentally to understand the far from equilibrium coarsening phenomena and practically because the order affects the functional properties of the systems.

In BCP self-assembly, the nanostructures emerging from the phase separation are encoded in the molecular composition of the constituent polymer chains. BCPs consisting of two covalently end joined polymeric blocks are single component systems as the chemically different blocks cannot macrophase separate [13]. The covalent bond between the two blocks constrains the system to microphase segregate. The chain composition (f) determines primarily the equilibrium morphology of the ordered phase, moving from lamellae to cylinders, gyroids, and spheres, increasing the disproportion between the two chains [14]. A 2D hexagonal structure results from a single layer matrix of spherical domains or from thin films comprising domains of cylinders perpendicularly oriented with respect to the substrate [15]. The degree of polymerization (N), i.e., the number of monomeric units in the polymer chain, sets the characteristic dimensions: diameter (d) of the domains and periodicity (L_0) between the domains. The Flory-Huggins parameter (χ) quantifies the thermodynamic interaction between the two distinct monomeric units and accounts for the change in local free energy. The BCP free energy, that determines the equilibrium state of the system, is composed by an entropic contribution [$\Delta S/(1/N)$] and by an enthalpic one ($\Delta H/\chi$). The overall segregation strength is hence governed by χN. With positive χ, the competition between ΔH reduction, because of the local segregation between the different blocks, is counterbalanced by the ΔS decrement due to the localization of the interface between the blocks and to the stretching of the chains. When $\chi N \ll 10$, the dominant ΔS drives the system in a spatially homogenous phase. At $\chi N \approx 10$, the two opposite effects are balanced, defining the order-disorder transition (ODT) boundary in the phase diagram. For $\chi N \gg 10$, ΔH dominates and microphase segregation appears [13]. According to this picture, χN establishes the minimum attainable size of the domains in the phase separated system [16]. The thermodynamic driving force for the phase separation increases with N or, when χ is temperature (T) dependent, decreasing T. However, for high N, or low T, the ordering kinetics is limited by the reduced diffusivity of the system. The real ordering process results from the balance between the slow kinetics and the enhanced thermodynamic [8].

Due to their potential applications as advanced tools for nanofabrication, accurate and reliable approaches have been developed to control BCP self-assemblies [17–19]. This broad experimental knowledge makes BCPs appealing as model systems for uncovering the interplay between thermodynamic driving forces and kinetic barriers during the ordering process. Mesoscopic order results from the competition between a segmental short-range attractive and a chain long-range repulsive interaction [6,12,20,21]. Experimentally, BCP thin films

*gabriele.seguini@mdm.imm.cnr.it
†michele.perego@mdm.imm.cnr.it

TABLE I. Molecular weight (M_n), polydispersity index (PDI), degree of polymerization (N), styrene fraction (f_S), MMA degree of polymerization (N_{MMA}), annealing temperatures (T_A), reference T_A for TTS, diameter (d), periodicity (L_0), growth exponent (ϕ), and activation enthalpy (H_A) for the different BCPs.

M_n (kg/mol)	PDI	N	f_S	N_{MMA}	T_A (°C)	T_A (TTS) (°C)	d (nm)	L_0 (nm)	ϕ	H_A (kJ/mol)
47.5	1.07	461	0.74	125	160–240	180	12.5 ± 0.5	26.5 ± 0.5	0.32 ± 0.02	65 ± 5
53.8	1.07	523	0.69	168	160–240	180	13.0 ± 0.1	28.8 ± 0.5	0.34 ± 0.01	63 ± 5
67.1	1.09	652	0.69	210	190–270	190	17.0 ± 0.1	35.0 ± 1.0	0.17 ± 0.01	42 ± 3
82.0	1.07	797	0.69	250	190–290	190	19.0 ± 0.2	42.9 ± 0.7	0.13 ± 0.01	32 ± 2
101.5	1.08	988	0.67	335	190–290	190	22.7 ± 1.5	47.0 ± 1.0	0.10 ± 0.01	28 ± 1
132.0	1.11	1281	0.73	355	190–270	190	28.6 ± 1.6	59.0 ± 4.0	0.08 ± 0.01	26 ± 1

are prepared by a spin-coating procedure, where a solvent mediates the unfavorable interactions between the blocks. Solvent evaporation prevents the motion of the chains and the resulting spin-coated polymer film is frozen in a metastable state [22,23]. An anneling step is necessary to release this phase. The temperature processing window for microphase ordering is comprised between the glass transition temperature (T_G) and the onset of thermal degradation of the polymer chains [24]. Thermal annealing (TA) [25], increasing T, or solvent vapor annealing (SVA) [23,26], adding a solvent, facilitates the phase separation and the defect annihilation through the increased chain mobility [26]. TA and SVA processes are thermodynamically equivalent as they can be mapped on the BCP phase diagram considering the solvent effect as a kinetic (plasticization, reduction of T_G) or as a thermodynamic effect (dilution, reduction of χ) [14]. A rapid TA (RTA) approach provides the possibility to reach target T in very short time, even though not instantaneous, taking advantage of the residual solvent trapped in polymer film to boost the chain mobility and speed up the ordering process [27,28]. This solvent-assisted RTA (SARTA) treatment was demonstrated to be a valuable tool to probe the ordering process in phase separated BCP thin films [27–32]. In more detail, the RTA treatment is composed of three parts, a heating ramp, an isothermal step at constant T_A, and a cooling ramp. For heating rates equal to or higher than 18 °C/s, the final level of order of the system is mainly determined by the isothermal step, with negligible contribution of the heating ramp. On the other hand, the cooling step is fixed by the machine recovery time [32].

This paper aims to experimentally determine the ordering kinetics dependence on χN in a 2D hexagonal pattern of strongly segregated cylinder-forming polystyrene-*block*-poly (methyl methacrylate) (PS-*b*-PMMA) BCP thin films. To promote perpendicular orientation of the domains in the PS-*b*-PMMA BCP thin films, a poly (styrene-*random*-methyl methacrylate) [P(S-*r*-MMA)] random copolymer (RCP) (molecular weight, $M_n = 69$ kg/mol, Styrene fraction, $f_s = 0.61$, polydispersity index, PDI = 1.19) was grafted (RTA: $T = 310$ °C, $t = 60$ s) on a hydroxyl terminated Si surface to form a neutral ≈19-nm-thick brush layer. This thick RCP brush layer provides a reservoir of embedded solvent [29,30,33] able to sustain the ordering process in the phase separated PS-*b*-PMMA film over several decades of time during the SARTA treatment [29]. The all-organic PS-*b*-PMMA BCP exhibits a $\chi_{S\text{-}MMA}$ parameter that is weakly dependent on T, because the entropic contribution (0.021) is much larger than the enthalpic one (3.2/T) [34–36]. This enables studies of the ordering process over a wide range of T keeping χ almost constant and modulating χN, i.e., the driving force for the phase separation, by changing N [34,37]. Asymmetric PS-*b*-PMMA BCPs with $f_S \approx 0.7$, PDI $\leqslant 1.11$, and different N ranging from 461 to 1281 (Table I) were spinned in toluene solution to obtain a ≈30-nm-thick layer. The ordering process in the BCP thin films was systematically studied considering different combinations of annealing time (t_A) and temperature (T_A). For each T_A, typically comprised between 160 and 290 °C, grain coarsening evolution was assessed at $t_A = 1$, 9, 90, and 900 s. Slightly different T_A ranges were defined for each BCP depending on N [31]. Heating rate was fixed at 18 °C/s for all the samples. Irrespective of the annealing parameters, increasing N, d varies from 12.5 to 28.6 nm while L_0 changes from 26.5 to 59.0 nm following the law $L_0/N^{2/3}$ [31]. The 2/3 exponent sets the investigated BCPs in the strong segregation limit (SSL), thus resulting in sharp interfaces between the segregated blocks [38]. For $N < 461$, χN approaches the critical value corresponding to ODT, preventing the possibility to investigate ordering process over a proper range of (T_A, t_A) values [24].

Surface morphology of the self-assembled BCPs was investigated by scanning electron microscopy (SEM) images. [31]. Because of the probe depth of electrons, the top-down SEM gives real-space information of the BCP domains only near the free surface. Considering the thickness of the BCP film, the cylindrical domains are expected to propagate throughout the entire film depth [31]. Representative high-magnification SEM images at each (T_A, t_A) combination for different BCPs are reported in Supplemental Material (SM), Figs. 1–6 [39]. The order of the 2D hexagonal pattern was quantified by measuring the correlation length (ξ) using Delaunay triangulation to detect the pattern orientation in SEM images [14], providing information over an area that is much larger than the measured correlation length, as previously detailed in Ref. [29]. This procedure rules out possible finite-size effects, within the limits of this real-space method [14]. When $\xi > L_0$ ($1 < \xi < 2L_0$ and $\xi > 2L_0$ correspond to blue and green SEM images, respectively, in SM, Figs. 1–6) [39], the system, after the (rapid) early-stage phase separation, enters the (slow) late-stage coarsening regime [40]. In this regime, the average grain dimensions regularly increase their order as a function of the increased T_A or t_A for all the investigated N. At higher T_A and t_A, inhomogeneities begin to appear on the sample surface (see red SEM images in SM, Figs. 1–6) [39]. These samples were not considered for the quantitative evaluation of ξ evolution. For each (T_A, t_A) combination, average ξ values

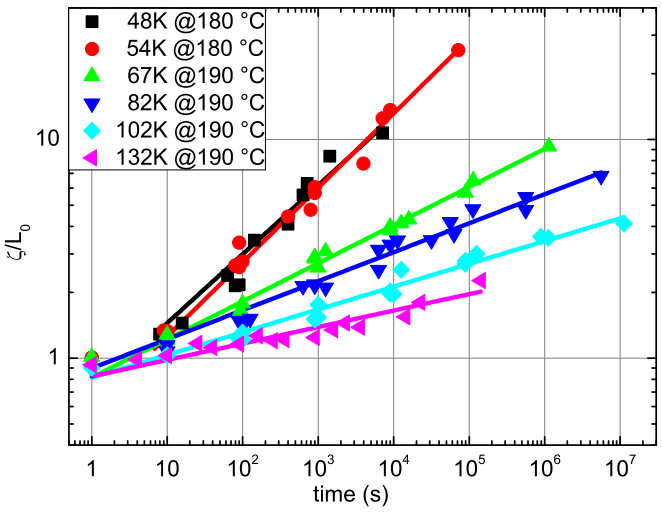

FIG. 1. Evolution of the correlation length normalized over the periodicity (ξ/L_0) as a function of the t_{EQ} after the TTS procedure for BCP of different N (461, 523, 652, 797, 987, and 1281). The slopes of the curves represent the growth exponent ϕ.

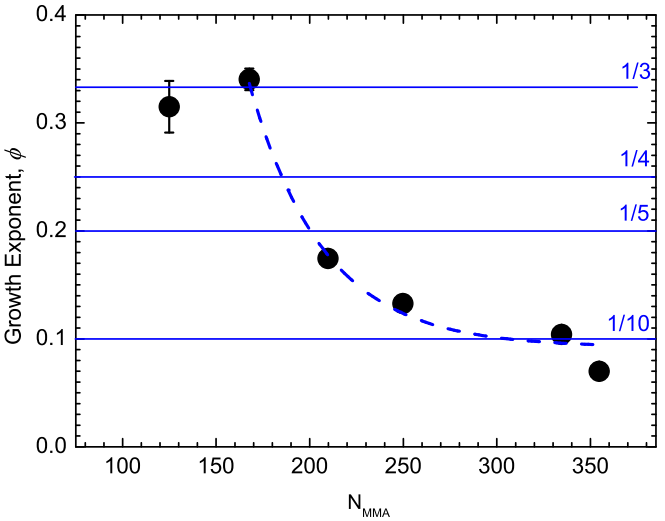

FIG. 2. Growth exponent ϕ as a function of N_{MMA}.

were obtained from the analysis of at least five SEM images acquired in different regions of the sample. The dispersion of the data was evaluated as the standard deviation from the average. The measured ξ value can be treated following the time-temperature superposition (TTS) procedure, to describe the ordering kinetics [29,32]. ξ as a function of t_A for different T_A are collected in a master curve at the reference T_A (Table I) versus an equivalent time (t_{EQ}) spanning over several decades. All the master curves can be fitted with a simple power law, irrespective of N (see SM, Figs. 7–12) [39]. This regular behavior confirms the pertinence of the TTS procedure and evidences a self-similar time evolution.

Figure 1 reports the evolution of ξ/L_0 as a function of t_{EQ} for different BCPs. All the ordering curves are normalized by dividing the grain dimension (ξ) by the inherent periodicity of the specific BCP (L_0). This evidences the number of ordered rows of the cylinder domains irrespective of N, i.e., of the physical dimensions of the domains [31]. ξ/L_0 curves follow a power law t^{ϕ}, with different ϕ values (from $\approx 1/3$ to $\approx 1/10$) depending on N (Table I). Interestingly ϕ is not constant within the cylindrical morphology but it is N dependent, that is, basically, it depends on the driving force for the phase separation [41]. ϕ results in $1/3$ for $N = 523$ and no further increase is observed decreasing N, suggesting $1/3$ as the maximum ϕ for strongly segregated standing cylinder domains resulting from BCP self-assembly. Increasing N, progressive reduction of ϕ is observed. Interestingly, a $\phi \approx 1/3$ value equals the growth exponent for systems with only attractive interaction that coarsen with a rate limiting step that is a diffusion limited mechanism [20,42]. Literature data for thermally treated standing cylinders in PS-*b*-PMMA thin films report $1/4$ for BCP with $N = 652$, consistent with our experimental results [43,44].

Figure 2 reports ϕ values as a function of N_{MMA}, i.e., the length of the smaller of the two blocks. For $N_{MMA} > 167$, ϕ decreases as a function of N_{MMA}, following an exponential decay:

$$\phi \sim e^{-\chi N_{MMA}} \quad (1)$$

where χ has a value of 0.028 ± 0.002, in excellent agreement with χ_{S-MMA} values reported in the literature [34,37]. This result indicates that the grain coarsening process is retarded with a barrier proportional to the segregation strength χN_{MMA}. Note that the exponent, which depends on both χ and N, in this specific BCP system is almost T independent. The ϕ value for $N_{MMA} = 125$ is much lower than expected according to the extrapolation of Eq. (1), suggesting that the exponential dependence on the thermodynamic variable χN_{MMA} holds only in the SSL, that is, for $\chi N_{MMA} = O(\chi N_{MMA}^{ODT})$, where monomeric unit segregation impedes chain diffusion across different grains. Chain diffusion in phase separated BCP follows the same exponential decay of ϕ as a function of χN_{MMA}, because of the thermodynamic penalty for the diffusion due to the increased localization of the chain with N [15,45–47]. Ohnogi and Shiwa [11] reported simulations showing that ϕ depends on the value of the noise strength. It becomes progressively larger increasing noise, moving from a value ≈ 0.15 at zero noise up to a limiting value just above ≈ 0.30. The noise strength corresponds to a diffusion at the microscopic scale [48] and it is proportional to T [6]. Sagui and Desai [20] evaluated the growth exponent for a system with competing interactions phase separated into the exagonal phase, finding a value of 0.29. The exponent decreases to 0.18 increasing the long range repulsion interaction [20,21]. Tripathi and Kumar [41] reported a similar slowdown of the coarsening for stripe patterns increasing the distance from the transition point. These literature results are perfectly consistent with data herein presented, considering the decrease of diffusivity occurring because of the progressive N increase. Additionally, Adland *et al.* [2] noted that for a continuous lattice pattern of spatially modulated phase such as BCPs, because the polymer chains can stretch changing the shape of the domains [8], the growth is limited by dissipation in the grain interior associated with lattice translation. Their simulations predict a ϕ value

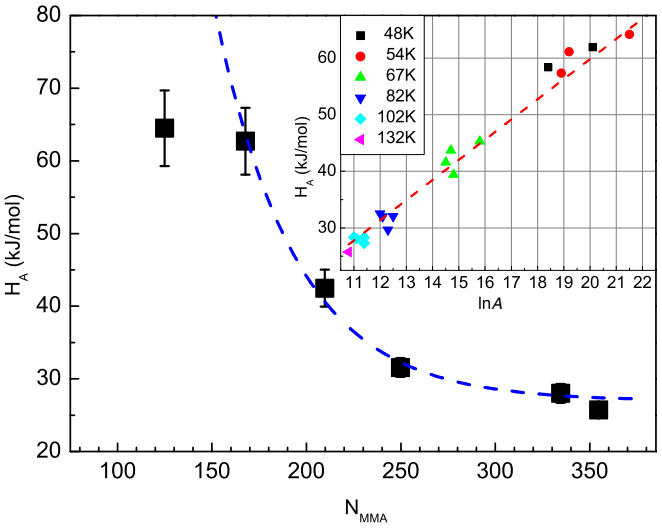

FIG. 3. Activation enthalpy H_A as a function of N_{MMA}. Inset: H_A as a function of the preexponential factor (ln$A$) of the Arrhenius plot corresponding to the activation entropy (S_A).

of 0.22 considering bulk dissipation. Differently, increasing T, i.e., increasing chain diffusivity, the reduction of the number of defects by dislocation reaction allows the grain to shrink with less rotation, reducing the contribution of the grain interior dissipation. A ϕ value of 0.35 is foreseen in case of minimized grain interior dissipation, consistent with our experimental findings for small N values.

To elucidate the kinetics of the grain coarsening process, the evolution of lnξ as a function of $1/T_A$ at different t_A has been investigated (see SM, Figs. 13–18) [39]. Experimental data can be fitted using an Arrhenius equation $\ln\xi = \ln A - H_A/(K_B T_A)$, where H_A corresponds to the activation enthalpy of an elementary step of the grain coarsening process, K_B is the Boltzmann constant, and A is the pre-exponential factor. The linear evolution of lnξ as a function of $1/T_A$ indicates that the grain coarsening process is a thermally activated process with a kinetic barrier. Limited variations of H_A with t_A have been observed for each N, resulting in a mean H_A value with limited dispersion for each specific BCP (Table I). Figure 3 reports the mean H_A values as a function of N_{MMA}. For $N_{\mathrm{MMA}} > 167$, H_A data follow an exponential decay as a function of N_{MMA}:

$$H_A \sim e^{-\chi N_{\mathrm{MMA}}} \tag{2}$$

where χ has a value of 0.024 ± 0.005, consistent with the χ value obtained by fitting ϕ data using Eq. (1) and data in the literature [34,37]. It is worth noting that, for grain coarsening of a standing hexagonal cylinder, Majewski and Yager [49] reported a value of 69 ± 23 kJ/mol for a 49-kg/mol ($N \approx 461$) BCP, and Ji *et al.* [43] reported 24–43 kJ/mol for a 67-kg/mol ($N = 523$) BCP, in perfect agreement with our results.

Present H_A values are much lower than free-energy barriers associated to topological defect creation [50–52]. Actually, topological defects in self-assembled BCP templates result from a collection of many molecules and they cannot be considered as equilibrium fluctuations around a perfectly ordered state. On the contrary, they correspond to nonequilibrium metastable states, kinetically frozen during phase separation and the initial stages of the self-assembling process [50–52]. The excess free energy (penalty) to create a defect is large and increases with χN. The corresponding equilibrium defect density is small and exponentially decreases with this penalty [37,50–52]. The free-energy barriers for defect removal are much lower than the excess free energy to create a defect. These free-energy barriers are of the same order of magnitude as the H_A values we measured for the grain coarsening process on unpatterned flat surfaces, but their evolution as a function of N follows an opposite trend compared to H_A [1,51].

The decrease in the grain coarsening kinetics and of the activation enthalpy with increasing N can be rationalized in the framework of the ubiquitous thermodynamic compensation effect [53]. The inset of Fig. 3 reports the relationship between H_A and ln$A$, i.e., the preexponent of the Arrhenius equation, that is related to the activation entropy S_A. The linear relationship indicates that these data follow the Meyer-Neldel (MN) rule [54,55], i.e., $\Delta S = \Delta H/T_{\mathrm{MN}}$, where T_{MN} is the MN temperature. In thermally activated processes, going from the metastable ground state to the activated one, the number of paths to the activated state supplied by the heat bath increases with H_A, resulting in an increase of entropy for the system. For $T > T_{\mathrm{MN}}$ an increase of H_A corresponds to a large positive change ΔS, lowering the free-energy barrier that limits grain coarsening. From another point of view, it has been shown that the compensation is a consequence of a balance between repulsive and attractive interactions [56]. From the slope of the linear fitting of the data in the inset of Fig. 3, T_{MN} is 428 K (155 °C). Considering that for these BCPs the reported mean bulk T_G of PS is ≈378 K (105 °C) and that of PMMA is ≈397 K (124 °C), it results that $T_{\mathrm{MN}} \approx 1.1 T_G$. Above T_G and below the scales of the domain size, blocks can be considered as liquid [15]. In this context, a value above $\approx 1.2 T_G$ sets the threshold where the inverse relationship between diffusivity and viscosity holds [57–60].

In conclusion, reported data demonstrate connections between the BCP equilibrium state and the ordering kinetics of the system. In this framework, a model system (PS-*b*-PMMA) along with a suitable process (SARTA) emerge as a platform for fundamental studies where a collection of various universal behavior can be simultaneously scrutinized. The small dependence on T of $\chi_{\text{S-MMA}}$ allows following the ordering process as a function of N, indeed using $1/N$ instead of T as a unique variable to modify the thermodynamic driving force that guides the system toward the equilibrium state and investigate the thermally activated kinetics of pattern formation in BCP thin films. The molecular architecture of the BCP encodes the characteristic dimensions (d, L_0) as well as the activation enthalpy (H_A) and the kinetics (ϕ) of the ordering process. Furthermore, the growth exponent data highlights two facts: the exponential decay with N_{MMA} and a maximum limiting value of 1/3 for BCP in the SSL. The former mimics the decrease of the diffusivity with N_{MMA}, highlighting that the grain coarsening process is limited by single chain diffusion. The latter sheds light on the mechanism of the ordering process in the general contest of the rate of decrease of the total excess grain boundary free energy in a polycrystal. Moreover, the linear dependence between H_A and S_A sets the system in the ubiquitous thermodynamic compensation rules where the

linear factor is correlated to the T_G of the BCP and it is the transition temperature to the activated coarsening state.

The authors acknowledge K. Sparnacci, V. Gianotti, and D. Antonioli (Università Del Piemonte Orientale, Italy) for their assistance in RCP synthesis; M. Alia [Consiglio Nazionale delle Ricerche—Institute for Microelectronics and Microsystems (CNR-IMM), Italy] for assistance in the experimental part; and T. J. Giammaria (CNR-IMM, Italy) and F. Ferrarese Lupi (Istituto Nazionale di Ricerca Metrologica, Italy) for fruitful discussion. This research has been partially supported by the project "IONS4SET" funded from the European Union's Horizon 2020 research and innovation program under Grant No. 688072.

[1] W. Li and M. Müller, Annu. Rev. Chem. Biomol. Eng. **6**, 187 (2015).
[2] A. Adland, Y. Xu, and A. Karma, Phys. Rev. Lett. **110**, 265504 (2013).
[3] A. D. Pezzutti, L. R. Gómez, M. A. Villar, and D. A. Vega, EPL **87**, 66003 (2009).
[4] F. A. Lavergne, D. G. A. L. Aarts, and R. P. A. Dullens, Phys. Rev. X **7**, 041064 (2017).
[5] W. T. M. Irvine, V. Vitelli, and P. M. Chaikin, Nature (London) **468**, 947 (2010).
[6] D. A. Vega, C. K. Harrison, D. E. Angelescu, M. L. Trawick, D. A. Huse, P. M. Chaikin, and R. A. Register, Phys. Rev. E **71**, 061803 (2005).
[7] M. R. Hammond, S. W. Sides, G. H. Fredrickson, E. J. Kramer, J. Ruokolainen, and S. F. Hahn, Macromolecules **36**, 8712 (2003).
[8] R. A. Segalman, A. Hexemer, R. C. Hayward, and E. J. Kramer, Macromolecules **36**, 3272 (2003).
[9] D. E. Angelescu, C. K. Harrison, M. L. Trawick, R. A. Register, and P. M. Chaikin, Phys. Rev. Lett. **95**, 025702 (2005).
[10] R. A. Segalman, A. Hexemer, and E. J. Kramer, Phys. Rev. Lett. **91**, 196101 (2003).
[11] H. Ohnogi and Y. Shiwa, Phys. Rev. E **84**, 051603 (2011).
[12] Y. Yokojima and Y. Shiwa, Phys. Rev. E **65**, 056308 (2002).
[13] F. S. Bates, Science **251**, 898 (1990).
[14] P. W. Majewski and K. G. Yager, J. Phys. Condens. Matter **28**, 403002 (2016).
[15] H. Yokoyama, Mater. Sci. Eng. R Reports **53**, 199 (2006).
[16] T. Xu, H. C. Kim, J. DeRouchey, C. Seney, C. Levesque, P. Martin, C. M. Stafford, and T. P. Russell, Polymer **42**, 9091 (2001).
[17] J. Frascaroli, S. Brivio, F. Ferrarese Lupi, G. Seguini, L. Boarino, M. Perego, and S. Spiga, ACS Nano **9**, 2518 (2015).
[18] H. Tsai, J. W. Pitera, H. Miyazoe, S. Bangsaruntip, S. U. Engelmann, C. C. Liu, J. Y. Cheng, J. J. Bucchignano, D. P. Klaus, E. A. Joseph, D. P. Sanders, M. E. Colburn, and M. A. Guillorn, ACS Nano **8**, 5227 (2014).
[19] L. Wan, R. Ruiz, H. Gao, K. C. Patel, and T. R. Albrecht, ACS Nano **9**, 7506 (2015).
[20] C. Sagui and R. C. Desai, Phys. Rev. Lett. **74**, 1119 (1995).
[21] C. Sagui and R. C. Desai, Phys. Rev. E **52**, 2822 (1995).
[22] S. P. Paradiso, K. T. Delaney, C. J. García-Cervera, H. D. Ceniceros, and G. H. Fredrickson, ACS Macro Lett. **3**, 16 (2014).
[23] S. Hur, G. Khaira, A. Ramírez-Hernández, M. Müller, P. F. Nealey, and J. J. de Pablo, ACS Macro Lett. **4**, 11 (2014).
[24] G. Seguini, T. J. Giammaria, F. Ferrarese Lupi, K. Sparnacci, D. Antonioli, V. Gianotti, F. Vita, I. F. Placentino, J. Hilhorst, C. Ferrero, O. Francescangeli, M. Laus, and M. Perego, Nanotechnology **25**, 045301 (2014).
[25] A. M. Welander, H. Kang, K. O. Stuen, H. H. Solak, M. Müller, J. J. De Pablo, and P. F. Nealey, Macromolecules **41**, 2759 (2008).
[26] I. P. Campbell, C. He, and M. P. Stoykovich, ACS Macro Lett. **2**, 918 (2013).
[27] F. Ferrarese Lupi, T. J. Giammaria, M. Ceresoli, G. Seguini, K. Sparnacci, D. Antonioli, V. Gianotti, M. Laus, and M. Perego, Nanotechnology **24**, 315601 (2013).
[28] M. Perego, F. Ferrarese Lupi, M. Ceresoli, T. J. Giammaria, G. Seguini, E. Enrico, L. Boarino, D. Antonioli, V. Gianotti, K. Sparnacci, and M. Laus, J. Mater. Chem. C **2**, 6655 (2014).
[29] G. Seguini, F. Zanenga, T. J. Giammaria, M. Ceresoli, K. Sparnacci, D. Antonioli, V. Gianotti, M. Laus, and M. Perego, ACS Appl. Mater. Interfaces **8**, 8280 (2016).
[30] K. Sparnacci, D. Antonioli, V. Gianotti, M. Laus, F. Ferrarese Lupi, T. J. Giammaria, G. Seguini, and M. Perego, ACS Appl. Mater. Interfaces **7**, 10944 (2015).
[31] F. Ferrarese Lupi, T. J. Giammaria, G. Seguini, F. Vita, O. Francescangeli, K. Sparnacci, D. Antonioli, V. Gianotti, M. Laus, and M. Perego, ACS Appl. Mater. Interfaces **6**, 7180 (2014).
[32] M. Ceresoli, F. G. Volpe, G. Seguini, D. Antonioli, V. Gianotti, K. Sparnacci, M. Laus, and M. Perego, J. Mater. Chem. C **3**, 8618 (2015).
[33] T. J. Giammaria, F. Ferrarese Lupi, G. Seguini, K. Sparnacci, D. Antonioli, V. Gianotti, M. Laus, and M. Perego, ACS Appl. Mater. Interfaces **9**, 31215 (2017).
[34] T. P. Russell, R. P. Hjelm, and P. A. Seeger, Macromolecules **23**, 890 (1990).
[35] T. P. Russell, Macromolecules **26**, 5819 (1993).
[36] Q. Tong and S. J. Sibener, Macromolecules **46**, 8538 (2013).
[37] I. P. Campbell, S. Hirokawa, and M. P. Stoykovich, Macromolecules **46**, 9599 (2013).
[38] K. Koo, H. Ahn, S.-W. Kim, D. Y. Ryu, and T. P. Russell, Soft Matter **9**, 9059 (2013).
[39] See Supplemental Material at http://link.aps.org/supplemental/10.1103/PhysRevMaterials.2.055605 for SEM images at each annealing time (t_A) and temperature (T_A) combination, master curves resulting from the time-temperature superposition procedure fitted with a power law, and Arrhenius plots, for each BCP.
[40] K. Glasner, Phys. Rev. E **92**, 042602 (2015).
[41] A. K. Tripathi and D. Kumar, Phys. Rev. E **91**, 022923 (2015).
[42] A. J. Bray, Adv. Phys. **51**, 481 (2002).
[43] S. Ji, C. Liu, W. Liao, A. L. Fenske, G. S. W. Craig, and P. F. Nealey, Macromolecules **44**, 4291 (2011).
[44] C. T. Black and K. W. Guarini, J. Polym. Sci. Part A: Polym. Chem. **42**, 1970 (2004).
[45] M. C. Dalvi, C. E. Eastman, and T. P. Lodge, Phys. Rev. Lett. **71**, 2591 (1993).

[46] K. A. Cavicchi and T. P. Lodge, Macromolecules **37**, 6004 (2004).
[47] T. P. Lodge and M. C. Dalvi, Phys. Rev. Lett. **75**, 657 (1995).
[48] T. Shinbrot and F. J. Muzzio, Nature (London) **410**, 251 (2001).
[49] P. W. Majewski and K. G. Yager, Soft Matter **12**, 281 (2015).
[50] H. Takahashi, N. Laachi, K. T. Delaney, S. M. Hur, C. J. Weinheimer, D. Shykind, and G. H. Fredrickson, Macromolecules **45**, 6253 (2012).
[51] W. Li, P. F. Nealey, J. J. de Pablo, and M. Muller, Phys. Rev. Lett. **113**, 168301 (2014).
[52] S.-M. Hur, V. Thapar, A. Ramírez-Hernández, G. Khaira, T. Segal-Peretz, P. A. Rincon-Delgadillo, W. Li, M. Müller, P. F. Nealey, and J. J. de Pablo, Proc. Natl. Acad. Sci. USA **112**, 14144 (2015).
[53] A. Yelon, B. Movaghar, and R. S. Crandall, Reports Prog. Phys. **69**, 1145 (2006).
[54] A. Yelon and B. Movaghar, Phys. Rev. Lett. **65**, 618 (1990).
[55] Hyung Ju Ryu, Q. Tong, and S. J. Sibener, J. Phys. Chem. Lett. **4**, 2890 (2013).
[56] J. F. Douglas, J. Dudowicz, and K. F. Freed, Phys. Rev. Lett. **103**, 135701 (2009).
[57] P. G. Debenedetti and F. H. Stillinger, Nature (London) **410**, 259 (2001).
[58] X. Wu, C. S. Liu, and K. L. Ngai, Soft Matter **10**, 9324 (2014).
[59] A. P. Sokolov and K. S. Schweizer, Phys. Rev. Lett. **102**, 248301 (2009).
[60] Y. J. Wang, M. Zhang, L. Liu, S. Ogata, and L. H. Dai, Phys. Rev. B **92**, 174118 (2015).